Conformations of Stilbene-like Species and New Method of Energy Partition

Zhong-Heng Yu,* Lin-Tong Li, Wei Fu, and Liang-Ping Li

Institute of Chemistry, Chinese Academy of Sciences, Beijing 100080, People's Republic of China

Received: August 13, 1997; In Final Form: December 10, 1997

To understand the nature of π-electron delocalization, while questioning the abnormally large twist angle of *N*-benzylideneaniline, we prepared four stilbene-like species, (4-X-Ph)-CH═N-Ar (Ar = 2-pyridyl, X = -Cl, $-NO_2$, $-N(Me)_2$; Ar = 2-pyrimidyl, X = $-NO_2$), and four ketenimine derivatives, $(4\text{-X-Ph})_2C{=}C{=}N\text{-(Ph-Y-4)}$ (Y = -H, X = -H; Y = $-NO_2$, X = -H; Y = $-NO_2$, X = -OMe; Y = $-N(Me)_2$, X = -H), and determined their crystal structures using X-ray diffraction. Our new procedure for constructing a complete fragment molecular orbital (FMO) basis set is described in detail. Based on our procedure, the Morokuma's energy partitioning provides, in the framework of ab initio SCF-MO computation at the STO-3G level, the various π and σ energies associated with the inter- and intrafragment interactions. The π-electron delocalization in the DPI state of stilbene-like species is found to be destabilization. The DPI state is most destabilized at the coplanar geometry, and its electronic energy is the highest of four hypothetical electronic states. The characteristics of the quantum mechanical resonance energy (QMRE), including its role with regard to chemical reactivities toward electrophile attack, depend upon the response of the σ framework to the π-electron delocalization. In the case of stilbene-like species, the QMRE is destabilizing. Conversely, the QMRE of benzene is stabilizing. However, it is the σ framework of benzene, rather than the π system itself, which is strongly stabilized by the QMRE, revealing that benzene is σ aromatic. The driving forces for the out-of-plane twist of stilbene-like species arise from the QMRE and the σ orbital interaction. The electron-withdrawing (−I) groups and the ring-nitrogen atoms seem to have an obvious influence upon the twist angle.

Introduction

It has been recognized as a cornerstone of the classical structure theory of organic chemistry that molecules with conjugated double bonds have a higher thermodynamic stability than isomeric compounds having isolated double bonds. The standard textbook explanation for this stability is given in terms of resonance interactions.[1] It is also one of the fundamental concepts that the maximum resonance energy results from the planarity of the π system.[1,2] However, the abnormally large twist angle of stilbene-like species seems to challenge the viewpoint of π resonance stabilization.

The marked dissimilarity in the electronic spectra of stilbene (STB, **1a**) and *N*-benzylideneaniline (NBA) has led to many theoretical and experimental studies and arguments in the past two or three decades, including studies employing infrared (IR) and a variety of nuclear magnetic resonance (NMR) studies, X-ray crystallography, and molecular orbital calculations.[3] The resonance stabilization is always used to interpret the effects of substituents on the conformations of NBA and its substituted derivatives.[4] Burgi and recent researchers ascribed the large twist angle ($\phi = 55°$) of NBA to the contact of nonbonded atoms such as the hydrogen on the -N═CH- and one of the ortho hydrogens on the aniline ring. The loss of the π-electron energy in the twisted geometry can be compensated for partly by the intramolecular charge transfer (CT-2) from the bridge nitrogen lone-pair electrons to the phenyl ring and by the decrease in steric hindrance;[5] these researchers expected, therefore, that if the nonbonded interaction was neglected, the π-electron transfer (CT-1) between the conjugated fragments was found to favor the planar conformation of NBA.[6] Burgi's conclusions appear to be questioned by the angles ϕ of stilbene-like species, especially by those (both up to 30°) of **1a** and azobenzene (**1d**) in the gas state,[7] and by those of the compounds listed in Table 1. (The phrase "stilbene-like species listed in Table 1" or "the molecules of type **1**" is often, hereafter, shortened to "STB-type **1**".)

In order to discern whether conjugation effect depends on conformation or results in a nonplanar geometry, we prepared the following eight compounds with less nonbonded contact such as that in NBA: (4-X-Ph)-CH═N-2-pyridyl (**1e**, X = -Cl; **1f**, X = $-NO_2$; **1g**, X = $(Me)_2N$-), 4-NO_2-Ph-CH═N-2-pyrimidyl (**1i**) and $(4\text{-X-Ph})_2C{=}C{=}N\text{-(Ph-Y-4)}$ (**2a**, X = -H, Y = -H; **2b**, X = -H, Y = $-NO_2$; **2c**, X = -MeO, Y = $-NO_2$; **2d**, X = -H, Y = $-N(Me)_2$) and determined their crystal structures using X-ray diffraction (see Table 1 and Figures 1−3).

The total molecular energies E^T, total electronic energies E_e, and total nuclear repulsion energies E_N, occurring in seven typical optimized geometries of each of seven STB-type **1** were calculated using the AM1 method.[12] In addition, the nuclear repulsion energies E_n between the aromatic ring and fragment Ar-Q═P- were obtained from the ab initio SCF-MO (self-consistent field molecular orbital) program. The nonbonded contact in **1e**−**1g** and **1i** (Figure 1) should be comparable to that in **2a**−**2d** (Figure 2), but the twist angles ϕ for the former are generally larger than those for the latter. Of all the molecules listed in Table 1, the theoretical angle ($\phi = 50°$) of **1i** is largest and the experimental angle ($\phi = 0.5°$) of **2a** is smallest. The data in Table 2 are especially noteworthy. These data show identically that the driving force for out-of-plane twist of STB-type **1** arises from the electron interaction, expressed in terms of E_e, rather than from the nuclear repulsion E_N and E_n. At the $\theta = 30°$ geometry of **1h**, for example, the absolute

* E-mail: yuzh@infoc3.icas.ac.cn. Fax: (10) 62569564 (Institute).

S1089-5639(97)02660-1 CCC: $15.00
Published on Web 02/25/1998

TABLE 1: Experimental and Theoretical Values (deg) of Twist Angles ϕ and α in Compounds of Types 1 and 2

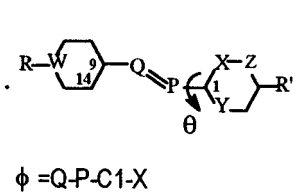

ϕ =Q-P-C1-X

α=P-Q-C9-C14 **1**

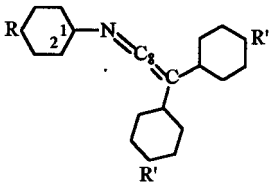

ϕ =C8-N-C1-C2 **2**

									twist angle ϕ		twist angle α	
compd	P	Q	X	Y	Z	W	R	R′	X-ray	AM1	X-ray	AM1
1a	CH	CH	CH	CH	CH	C	H	H	5[a]	27	5	27
1b	N	CH	CH	CH	CH	C	$N(Me)_2$	NO_2	41[b]	40	10	0
1c	N	CH	CH	CH	CH	C	NO_2	$N(Me)_2$	9[b]	15[e]	4	0
1d	N	N	CH	CH	CH	C	H	H	15[c]	15	15	15
1e	N	CH	N	CH	CH	C	Cl	H	15	13	6	3
1f	N	CH	N	CH	CH	C	NO_2	H	20	0	2	0.5
1g	N	CH	N	CH	CH	C	$N(Me)_2$	H	36	15[e]	7	0
1h	N	CH	CH	CH	N	C	H	H	46[d]	38	13.4	14
1i	N	CH	N	N	CH	C	NO_2	H	26	50	12	4.5
1j	N	CH	CH	CH	CH	N		H	21[d]	35[e]	8	2
2a							H	H	0.5			
2b							NO_2	H	16			
2c							NO_2	MeO	6.5			
2d							$N(Me)_2$	H	9.1			

[a] This value is from ref 8. [b] From ref 9. [c] From ref 10. [d] From ref 11. [e] Conformational space was sampled by varying θ in steps of 5°.

value (|−11 090.9611|eV) of E_e and value (9004.6837 eV) of E_N are greatest, and decrease as the molecular framework is distorted away from this geometry. Therefore, we cannot attribute the nonplanarity of STB-type **1** to the steric hindrance or to the crystal lattice force.[13] In molecule **2c** (Figure 2), the combination of the "pushing" and "pulling" actions, exerted by an electron-releasing (+M) group MeO- and an electron-withdrawing (−M) group -NO_2, respectively, should greatly benefit the CT-2 interaction between the nitrogen lone pair and phenyl ring A, and its twist angle $C_8-N_7-C_1-C_6$ should be larger than the angle (41°) in **1b**. At the least, it should be larger than that (16°) in **2b**. Contrary to expectation, the actual angle is only 9.2°. Nakai and collaborators found that the C_1-N_7 distance in several molecules such as **1c** (1.416 Å) and **1b** (1.398 Å) decreases with increasing CT-2 effect.[9] Accordingly, this distance should decrease in order of **1f**, **1i**, and **1g** and of **2d**, **2a**, **2b**, and **2c**, respectively. In fact, the bond length (1.439 Å) in **1i** is much longer than that (1.410 Å) in **1f**, and the experimental value (1.409 Å) in **1g** is almost equal to that in **1f** (Figure 1); of the four ketenimine derivatives, the distance (1.436 Å) in **2a** is longest and that (1.419 Å) in **2d** is shortest (Figure 2). Recently, our calculations have approximately shown that in the aniline molecule, the CT-2 interaction is destabilizing.[14] Accordingly, the nonplanarity of STB-type **1** cannot be explained in terms of the CT-2.

In this work, our procedure for constructing a complete fragment molecular orbital (FMO) basis set is described in detail. Morokuma's partition of the intermolecular SCF interaction energy,[15] denoted as M-SCF partition, is introduced into the intramolecular interaction, and it is used for analyzing the direct and indirect effects of the π-electron delocalization, respectively, on the π system itself and the σ frame in an effort to gain insight into the nature of the π-electron delocalization. Meanwhile, it is also applied to the σ interactions in order to search for the unknown driving force and to probe the influence of the electron-withdrawing (−I) effect upon the twist angle.

Methods and Computational Details

Based on the most common definitions of the resonance energy (RE),[16] the RE is essentially associated with the local interaction between double bonds. Inevitably, this interaction influences the original characteristics of the double bonds, including the observed and calculable changes in their bond lengths and bond orders, and also including the disturbance to their original π energies.[17] The geometric data in Figure 3, for example, indicate that the lengths of the bonds N_7-C_8 and C_1-C_6 are changed as the bond C_1-N_7 is lengthened from 1.405 to 1.411 Å with the rotation of fragment A about the C_1-N_7. Accordingly, the fundamental problems in the energy partitioning are how to calculate, reasonably and directly, the π energies occurring in a conjugated molecule and its corresponding hypothetical structures with the localized π systems, and how to evaluate the effects of the π-electron delocalization on the σ framework. In this sense, the perturbation molecular orbital (PMO) method should be more reasonable and valuable. It is prerequisite for the PMO analysis that the symmetric (σ) and antisymmetric (π) FMOs are thoroughly separated. It is easy when and only when the geometry of a molecule is planar.[18] However, STB-type **1** are not planar. In this case, the M-SCF method based on our new procedure becomes a useful instrument for partitioning total electronic energy. Our procedure provides a complete FMO basis set for the M-SCF partition.

According to the PMO theory[19] and based on the fact that in STB-type **1** both twist angles ϕ and α are not equal to 0° or 180°, we can consider a nonplanar molecule *N*-phenylmethylene-3-pyridineamine (**1h**), for example, as three planar opened-shell fragments, phenyl fragment (A), imine group -CH═N- (B), and 3-pyridyl fragment (C), i.e., A−B−C dissection as shown in Figure 4.

Figure 5 displays a thermodynamic cycle for the orbital interactions in STB-type **1**. It shows the symbols for the π- and σ-electronic energies in the following hypothetical states: the full localized state denoted as FUL; the state, denoted as DPI, with a delocalized π system and localized σ frameworks;

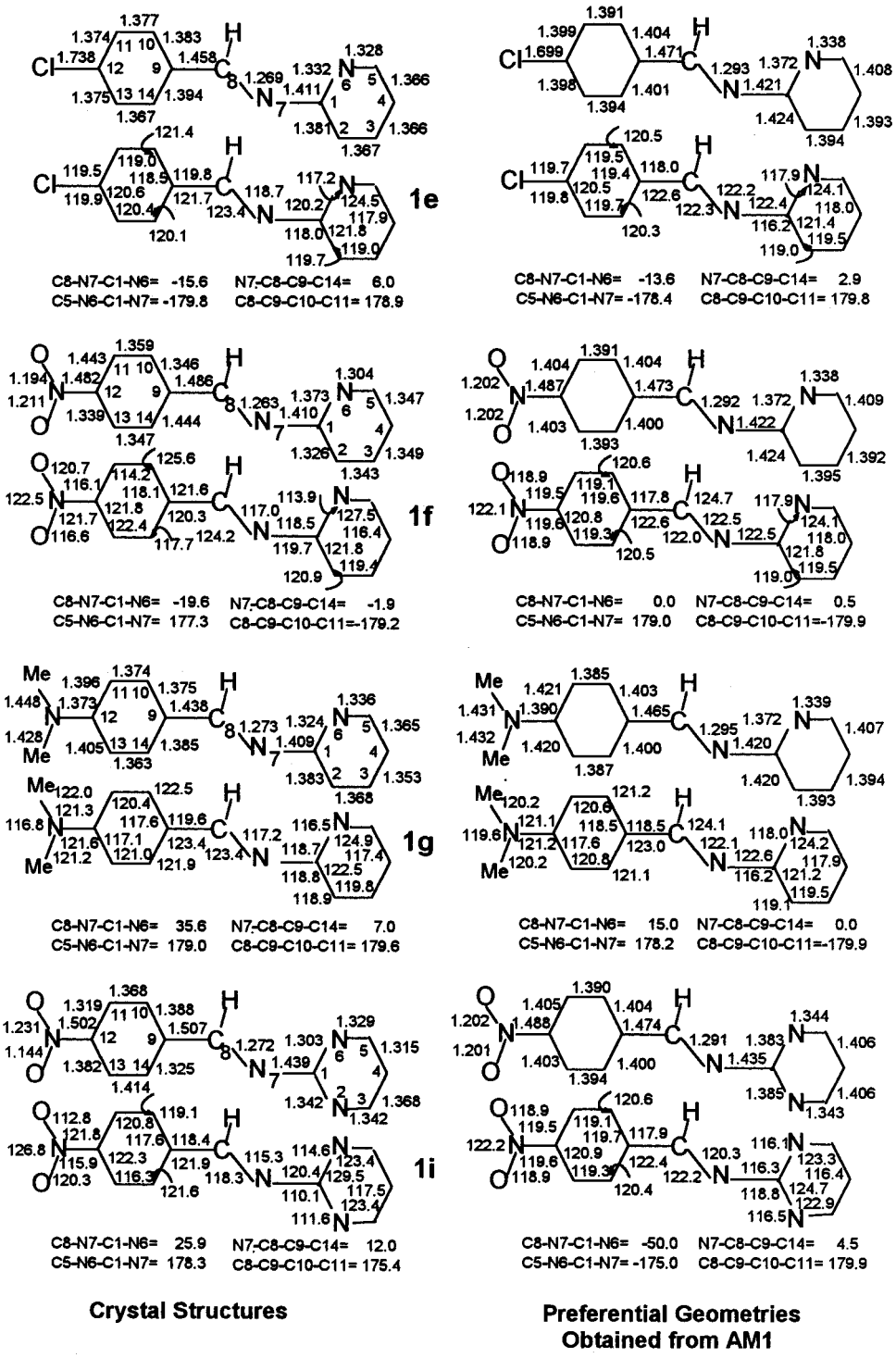

Figure 1. Experimental and theoretical geometric data of four stilbene-like molecules.

the DSI state with delocalized σ frameworks and localized π systems; the full delocalized state denoted as FUD. Figure 5 also contains a set of definitions of the various energy differences that will be used consistently in this work. For simplicity, these energy differences are expressed by the following general formulas:

$$\Delta E_{\pi}^{(\lambda,\rho)} = \Delta E_{ab+bc+ca}^{(\lambda,\rho)-\pi} + \Delta E_{a+b+c}^{(\lambda,\rho)-\pi} \qquad (1\text{-}1)$$

$$\Delta E_{\sigma}^{(\lambda,\rho)} = \Delta E_{ab+bc+ca}^{(\lambda,\rho)-\sigma} + \Delta E_{a+b+c}^{(\lambda,\rho)-\sigma} \qquad (1\text{-}2)$$

where the characters λ and ρ (λ, $\rho = \pi$, σ) in the superscript (λ,ρ) mean that the energy effects $\Delta E_{\pi}^{(\lambda,\rho)}$ and $\Delta E_{\sigma}^{(\lambda,\rho)}$ arise from the delocalization of the λ- and ρ-electrons; the characters π and σ in super- and subscripts denote that the energy effects are associated, respectively, with the π and σ orbital interactions. When $\lambda = \pi$ and $\rho = \pi$, eqs (1-1) and (1-2) become

$$\Delta E_{\pi}^{(\pi)} = \Delta E_{ab+bc+ca}^{(\pi)-\pi} + \Delta E_{a+b+c}^{(\pi)-\pi} \qquad (2\text{-}1)$$

$$\Delta E_{\sigma}^{(\pi)} = \Delta E_{ab+bc+ca}^{(\pi)-\sigma} + \Delta E_{a+b+c}^{(\pi)-\sigma} \qquad (2\text{-}2)$$

where $\Delta E_{\pi}^{(\pi)}$ and $\Delta E_{\sigma}^{(\pi)}$ are the energy differences between the DPI and FUL states. Two terms in the right side of eq (2-1)

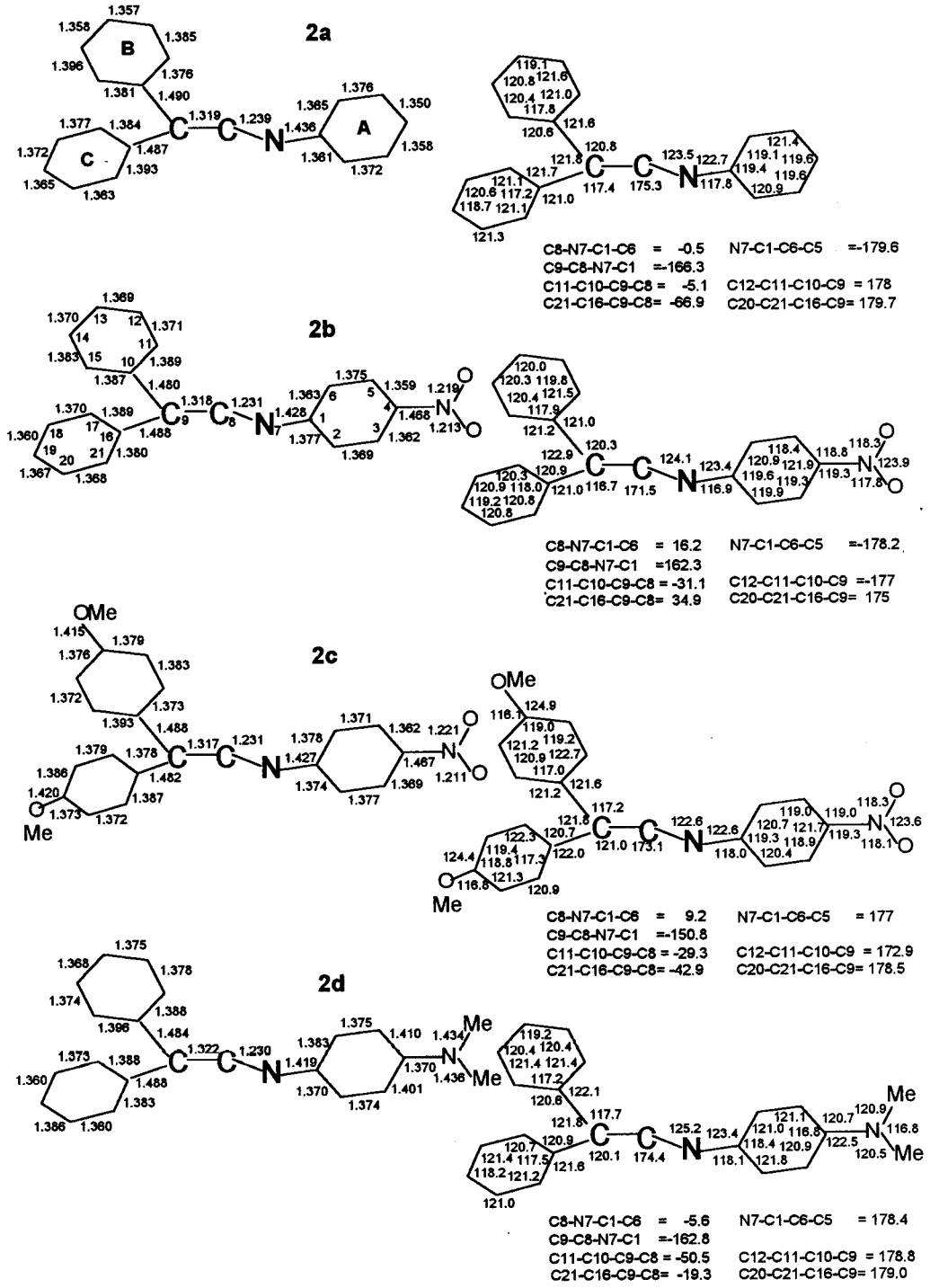

Figure 2. Crystallographic data of four ketenimine derivatives.

are the energy components associated, respectively, with the inter- and intrafragment interactions, and are given as

$$\Delta E^{(\pi)-\pi}_{ab+bc+cb} = \Delta E^{(\pi)-\pi}_{ab} + \Delta E^{(\pi)-\pi}_{bc} + \Delta E^{(\pi)-\pi}_{ca} \quad (2\text{-}3)$$

$$\Delta E^{(\pi)-\pi}_{a+b+c} = \Delta E^{(\pi)-\pi}_{a} + \Delta E^{(\pi)-\pi}_{b} + \Delta E^{(\pi)-\pi}_{c} \quad (2\text{-}4)$$

where

$$\Delta E^{(\pi)}_{a} = E^{(\pi)-\pi}_{a} - E^{(\mathrm{o})-\pi}_{a},\ \Delta E^{(\pi)}_{b} = E^{(\pi)-\pi}_{b} - E^{(\mathrm{o})-\pi}_{b},\ \Delta E^{(\pi)}_{c} = E^{(\pi)-\pi}_{c} - E^{(\mathrm{o})-\pi}_{c} \quad (2\text{-}5)$$

In the case of STB-type **1**, $|\Delta E^{(\pi)-\pi}_{ac}| < 10^{-3}$; hence, eq (2-3) is often written as

$$\Delta E^{(\pi)-\pi}_{ab+bc} = \Delta E^{(\pi)-\pi}_{ab} + \Delta E^{(\pi)-\pi}_{bc} \quad (2\text{-}6)$$

In this work, the energy components such as those in eqs (2-3)−(2-6) are often written as the general forms $\Delta E^{(\pi)-\lambda}_{pq}$ and $\Delta E^{(\pi)-\lambda}_{p}$ where $p, q = a, b, c$; $p \neq q$; $\lambda = \pi, \sigma$). In this case, the subscript pq and the character λ in the superscript $(\pi)-\lambda$ mean that the $\Delta E^{(\pi)-\lambda}_{pq}$ is associated with the λ orbital interactions between fragment P and Q (P, Q = A, B, C; P ≠ Q), and the subscript p denotes a energy effect $\Delta E^{(\pi)-\lambda}_{p}$ occurring in fragment P. In eq (2-5), the character o in the superscript (o) denotes that the $E^{(\mathrm{o})-\lambda}_{p}$ ($p = a, b, c$; $\lambda = \pi, \sigma$) is a λ electronic

TABLE 2: Total Molecular Energy E^T, Total Electronic Energy E_e, Total Nuclear Repulsion E_N, Nuclear Repulsion E_n (hartrees) between Fragments C and A + B, and Their Changes with Rotation of Fragment C (Energy in eV except for E_n)[a]

	$\theta = 0°$	$\theta = 5°$	$\theta = 10°$	$\theta = 30°$	$\theta = 50°$	$\theta = 70°$	$\theta = 90°$
				1a			
E^T	−1 956.3956	−1 956.3965	−1 956.3988	−1 956.4010	−1 956.3544		
E_e	−10 866.6455	−10 867.0250	−10 868.0638	−10 874.0003	−10 871.0929		
E_N	8 910.2499	8 910.6289	8 911.6649	8 917.5993	8 914.7384		
E_n	229.3696	229.3942	229.4682	229.9104	229.8220		
				1b			
E^T	−3 383.8153	−3 383.8150	−3 383.8191	−3 383.8376	−3 383.8378	−3 383.8211	
E_e	−20 354.9945	−20 355.6694	−20 356.3679	−20 362.3796	−20 360.1906	−20 351.4668	
E_N	16 971.1792	16 971.8534	16 972.5488	16 978.5420	16 976.3527	16 967.6457	
E_n	381.1377	381.1843	381.2470	381.7394	381.5754	380.8868	
				1d			
E^T	−2 085.5479	−2 085.5481	−2 085.5484	−2 085.5425	−2 085.5071	−2 085.4587	−2 085.4424
E_e	−11 110.8509	−11 110.8661	−11 110.9009	−11 111.6857	−11 111.8174	−11 108.9611	−11 107.4265
E_N	9 025.3029	9 025.3181	9 025.3525	9 026.1432	9 026.3103	9 023.5024	9 021.9545
E_n	237.0091	237.0092	237.0093	237.0371	237.0132	236.8095	236.6407
				1e			
E^T	−2 446.2838	−2 446.2839	−2 446.2841	−2 446.2803	−2 446.2559	−2 446.2068	
E_e	−12 559.3338	−12 559.3430	−12 559.5186	−12 560.4603	−12 560.3311	−12 557.6144	
E_N	10 113.0499	10 113.0591	10 113.2345	10 114.1800	10 114.0752	10 111.4076	
E_n	272.0361	272.0402	272.0553	272.1561	272.1461	271.8893	
				1f			
E^T	−2 917.0114	−2 917.0114	−2 917.0113	−2 917.0062	−2 916.9803		
E_e	−15 549.8119	−15 549.8462	−15 549.9552	−15 551.1046	−15 551.0171		
E_N	12 632.8005	12 632.8348	12 632.9439	12 634.0984	12 634.0368		
E_n	284.5411	284.5444	284.5526	284.6605	284.6523		
				1h			
E^T	−2 086.2632	−2 086.2643	−2 086.2665	−2 086.2773	2 086.2675	−2 086.2417	−2 086.2269
E_e	−11 087.7973	−11 087.8483	−11 088.1340	−11 090.9611	−11 089.0204	−11 082.1533	−11 078.3659
E_N	9 001.5341	9 001.5840	9 001.8675	9 004.6837	9 002.7529	8 995.9116	8 992.1390
E_n	235.6215	235.6290	235.6588	235.9209	235.7749	235.1954	234.8701
				1i			
E^T	−2 981.5947	−2 981.5953	−2 981.5982	−2 981.6182	−2 981.6315		
E_e	−15 656.0401	−15 656.1216	−15 656.2985	−15 658.3358	−15 658.4500		
E_N	12 674.4455	12 674.5263	12 674.6976	12 676.7176	12 676.8184		
E_n	286.1286	286.1398	286.1591	286.3514	286.3859		

[a] The starting geometry of each molecular conformation was taken from its crystal structure. The conformational space was sampled by varying θ in steps of 5° for $0° < \theta < 90°$. At each point a full optimization was carried out under the condition that all the ring atoms in each of two aromatic ring were kept coplanar.

energy in the FUL state of fragment P. In eq (2-2), the energy effect $\Delta E_\sigma^{(\pi)}$ is the response of the σ framework to the delocalization of the π-electrons and it arises from the effects of the π-electron delocalization on the $\sigma-\pi$ space interactions expressed in terms of the Coulomb $J_{\sigma\pi}$ and exchange $K_{\sigma\pi}$ integrals. In the M-SCF scheme, the energy components $\Delta E_{pq}^{(\pi)-\lambda}$ and $\Delta E_p^{(\pi)-\lambda}$ are obtained from the following general expressions:

$$\Delta E_{pq}^{(\pi)-\lambda} = \sum_{i,j}^{\lambda} (F_{ij}^{(\pi)-\lambda} + H_{ij}^{(\pi)-\lambda}) D_{ij}^{(\pi)-\lambda} \quad i \in \mathrm{P}, j \in \mathrm{Q} \qquad (3\text{-}1)$$

$$E_p^{(\pi)-\lambda} = \sum_{i,k}^{\lambda} (F_{ik}^{(\pi)-\lambda} + H_{ik}^{(\pi)-\lambda}) D_{ik}^{(\pi)-\lambda} \quad i, k \in \mathrm{P} \qquad (3\text{-}2)$$

$$E_p^{(\mathrm{o})-\lambda} = \sum_{i,k}^{\lambda} (F_{ik}^{(\mathrm{o})-\lambda} + H_{ik}^{(\mathrm{o})-\lambda}) D_{ik}^{(\mathrm{o})-\lambda} \quad i, k \in \mathrm{P} \qquad (3\text{-}3)$$

where **F**, **H**, and **D** are Fock, Hamiltonian, and density matrices respectively (a capital bold letter denotes, hereafter, a matrix over the complete FMO basis set); $F_{ij}^{(\pi)-\lambda}$, $H_{ij}^{(\pi)-\lambda}$, $D_{ij}^{(\pi)-\lambda}$ et al. are their respective elements. The various elements in eqs (3-1)−(3-2) are obtained from the RHF (restricted Hartree−Fock) computation, denoted as RHF$^\pi$-m in Figure 5, for the DPI state under the following conditions: in each SCF iteration, all the elements S_{ij} (the elements of the overlap integral matrix **S**) and F_{ij} ($i \neq j$) between the FMOs of the σ type are set equal to zero except four elements, $F_{sa,sb1}$, $S_{sa,sb1}$, $F_{sc,sb2}$, and $S_{sc,sb2}$. The subscripts *sa* and *sb*1 in $F_{sa,sb1}$ denote a pair of the singly occupied FMOs belonging, respectively, to two bonded fragments A and B, and the *sc* and *sb*2 (*sb*1 ≠ *sb*2) a pair of those belonging to fragments C and B. The conditional RHF computation, denoted as RHF$^\pi$-f, for the various elements in eq (3-3) was performed over the same complete FMO basis. In this computation, all the elements $S_{ij} = 0.0$ and $F_{ij} = 0.0$ ($i \neq j$) except the elements $F_{sa,sb1}$, $S_{sa,sb1}$, $F_{sc,sb2}$, and $S_{sc,sb2}$. In the conditional RHF computation, denoted as RHF$^\sigma$-m, for the various elements in the DSI state, all the F_{ij} and S_{ij} ($i \neq j$) between the FMOs of the π type are set equal to zero. The RHF-T computation for the elements, such as $F_{ij}^{(\sigma,\pi)-\lambda}$, $H_{ij}^{(\sigma,\pi)-\lambda}$, and $D_{ij}^{(\sigma,\pi)-\lambda}$, in the FUD state was performed under the constraint, a fundamental requirement for every type of conditional RHF computation, that all the F_{ij} and S_{ij} between the π and σ FMOs are set equal to zero. All the conditions employed in each of four types of the conditional RHF computations ensure that the molecular orbitals (MOs) of the π type are thoroughly separated from those of the σ type.

The complete FMO basis set, in which all FMOs have correct electron occupancies, consists of CDF-MOs (closed-shell de-

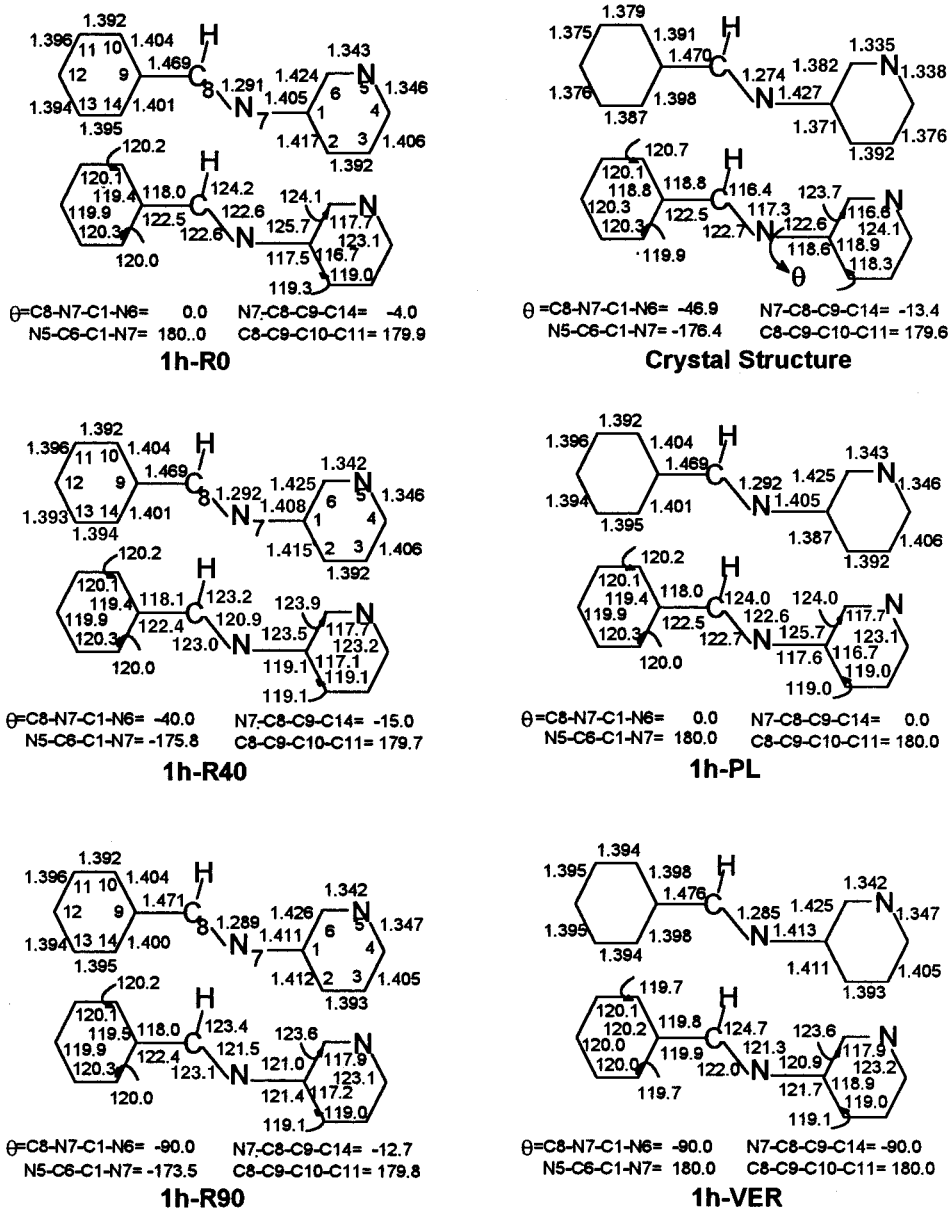

Figure 3. The crystal structure of **1h**, and its rotational geometries **1h-R0**, **1h-R40**, **1h-R90**, **1h-PL**, and **1h-VER** obtained from AM1.

localized FMOs) and singly occupied OLF-MOs (opened-shell localized FMOs). The construction of this basis set is a three-step procedure: (i) three basis sets from their respective planar fragment molecules (PFM), (ii) transformation of the basis set for the PFM into that for the corresponding nonplanar fragment molecule, and (iii) the formation of a complete basis set for the optimized geometry of a molecule by the superposition of three basis sets belonging, respectively, to fragments A, B, and C.

Construction of a Complete FMO Basis Set. According to the Whangbo−Schlegel−Wolfe−Kost (WSW-K) procedure,[20] i.e., a conditional UHF (unrestricted Hartree−Fock) computation for the composite system such as **1h** followed by the Kost's localization, three groups of OLF-MOs can be characterized by the following expressions:

$$\psi_{ai} = \sum_{k=1}^{na} a_{ki}\phi_k + \sum_{m=na+1}^{na+nb} a_{mi}\phi_m + \sum_{n=na+nb+1}^{N} a_{ni}\phi_n \quad (4\text{-}1)$$

$$\psi_{bj} = \sum_{k=1}^{na} a_{kj}\phi_k + \sum_{m=na+1}^{na+nb} a_{mj}\phi_m + \sum_{n=na+nb+1}^{N} a_{nj}\phi_n \quad (4\text{-}2)$$

$$\psi_{cl} = \sum_{k=1}^{na} a_{kl}\phi_k + \sum_{m=na+1}^{na+nb} a_{ml}\phi_m + \sum_{n=na+nb+1}^{N} a_{nl}\phi_n \quad (4\text{-}3)$$

where the atomic orbitals (AOs) ϕ_k ($k = 1, 2, ..., n_a$) ∈ A, ϕ_m ($m = n_a + 1, ..., n_a + n_b$) ∈ B, and ϕ_n ($n = n_a + n_b + 1, ..., N$) ∈ C; a_{ki}, a_{mi}, and a_{ni} are their coefficients. In our new procedure, the first sum term in eq (4-1) , i.e., a set of the OLF-MOs ψ_{ai} for the isolated fragment A, is obtained indirectly from a planar fragment molecule, denoted as FM-A in Figure 4b, using the WSW-K procedure. The FM-A resulted from the replacement of the 3-pyridyl-N═CH- group (B + C) in **1h** with a hydrogen atom denoted as H_r while all the bond angles and bond lengths were kept unchanged with the exceptions that the value of 1.0 Å was imposed on the length of the C_9-H_r bond and the dihedral angle $H_r-C_9-C_{10}-C_{11}$ was set equal to 180°. The 1s AO of the H_r, denoted as ψ_H, is an excellent singly occupied σ FMO, and the formation of the FM-A simplifies the localization procedure greatly. However, the dihedral angles, such as the $C_8-C_9-C_{10}-C_{11}$ and $N_7-C_1-C_2-C_3$ in Figures 1 and 3, are generally less than 180°. Therefore, it is necessary for the OLF-MOs of the σ type to be localized once more. In the second

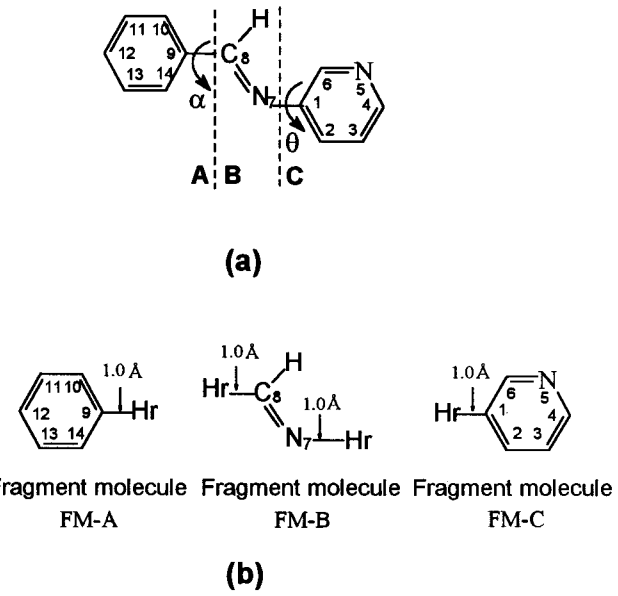

Figure 4. (a) The dissection way and the numbering system in *N*-phenylmethylene-3-pyridineamine (**1h**). The A−B−C dissection of **1h** into a phenyl fragment (A), an imine group (B), and a 3-pyridyl fragment (C). (b) Formation of the corresponding fragment molecules denoted as FM-A, FM-B, and FM-C.

localization, all the π OLF-MOs are kept unchanged, and the atomic overlap integral matrix **s** used in Kost's localization is from a nonplanar fragment molecule denoted as NFM-A. The only difference in the geometry between the FM-A and the NFM-A occurs in the angle $H_r-C_9-C_{10}-C_{11}$. In the case of the NFM-A, this angle is set equal to the $C_8-C_9-C_{10}-C_{11}$ in the optimized geometry of **1h**.

However, the Kost's localization fails to ensure all the π OLF-MOs correct electronic occupancies. A conditional RHF computation, over the OLF-MOs basis set, for the NFM-A has to be performed after the Kost's localization. From this computation, a set of the CDF-MOs φ_{ai} is obtained under the following conditions: first, all the elements $F_{ij} = 0.0$ and $S_{ij} = 0.0$ ($i \in$ A, $j \in H_r$) except two elements $F_{sa,H}$ and $S_{sa,H}$ between a pair of singly occupied OLF-MO ψ_{sa} and ψ_H; second, all the intrafragment elements $F_{sa,ai}$ and $S_{sa,ai}$ ($sa \neq ai$) and those between the π and σ OLF-MOs are set equal to zero. A set of the CDF-MOs and a singly occupied OLF-MO ψ_{sa} form a FMO basis set Φ_{ai} for fragment A. All Φ_{ai} have now correct electronic occupancies, and the π type of Φ_{ai} has been thoroughly separated from the σ type. A FMO basis set Φ_{bj} for fragment B and that Φ_{cl} for fragment C are obtained in a similar way. In the case of fragment B, there are two singly occupied OLF-MOs ψ_{sb1} and ψ_{sb2}. A singly occupied OLF-MO for fragment C is denoted as ψ_{sc}. At last, according to the characteristics as shown in eqs (4-1)−(4-3), a complete FMO basis set is formed by the superposition of three basis sets, Φ_{ai}, Φ_{bj}, and Φ_{cl}. In the meantime, all the coefficients corresponding to those a_{mi}, a_{ni}, a_{kj}, a_{nj}, a_{kl}, and a_{ml} in eqs (4-1)−(4-3) are set equal to zero.

In the case of larger molecules such as **1a**−**1j**, the calculations involving larger basis sets such as 6-31G et al. are extremely costly. In this work, the complete FMO basis set and the various orbital interaction energies were constructed and calculated using the ab initio SCF-MO computation program at the STO-3G level. The various rotational geometries were optimized using AM1. It should be stressed that during the period of any ab initio SCF iteration, the geometries of a molecule, its fragments and fragment molecules were no longer optimized.

Results and Discussion

Geometry Optimization. In our practical calculations, the rotational geometries of each of STB-type **1** were optimized using the various semiempirical calculations such as AM1, MNDO, MINDO/3, and PM3.[12] Our practical calculations and recent literature show that the AM1 method appears to be most suitable.[3,21] However, AM1 cannot treat correctly all the molecules. In fact, the abnormal difference in the twist angle ϕ between the experiment and AM1 calculation occurs in molecule **1f**. According to the energy data in Table 2, it may result from its rather flat potential energy.

The starting geometry of each molecular conformation was taken from the crystal structure, and the geometry optimizations for the various rotational conformers were experimentally carried out under the following two models: (i) the full optimization (Model I); (ii) all the dihedral angles are kept to be 0° or 180° (Model II). In addition, the H and ring atoms in each of two aromatic rings were kept on same plane, and the twist angle θ in a given rotational conformer was kept unchanged in above two models. Our practical calculations show that of all the dihedral angles, only the angle $P-C_1-X-Z$ has the greatest effect on the preferential geometry, and a larger angle θ corresponds generally to a larger deviation of the angle N_7-C_1-X-Z (X, Z = C, N) from 180° (see Figures 1−3). Therefore, the whole aromatic ring with a substituent group such as $-NO_2$, $-NH_2$, or -Cl can be considered approximately as a planar fragment, which will greatly simplify our computational procedure.

When $\alpha \neq 0$ and $\theta \neq 0$, there should be eight types of the FMO interactions. However, the $\sigma-\pi$ interaction results in the mixture of the σ and π FMOs and will not be considered here.

***π*-System Is Most Destabilized in the DPI State of Coplanar Geometry.** According to the definitions of the Coulomb and exchange integral matrices **J** and **K**, we have the following theoretical expressions for the elements in eqs (3-1)−(3-3).[22]

$$F_{ij}^{(\pi)-\lambda} = H_{ij}^{(\pi)-\lambda} + \sum_m \sum_n D_{mn}^{(\pi)-\lambda}[(ij,mn) - 1/2(im,jn)] \quad (5\text{-}1)$$

$$F_{ik}^{(\pi)-\lambda} = H_{ik}^{(\pi)-\lambda} + \sum_m \sum_n D_{mn}^{(\pi)-\lambda}[(ik,mn) - 1/2(im,kn)] \quad (5\text{-}2)$$

$$F_{ik}^{(o)-\lambda} = H_{ik}^{(o)-\lambda} + \sum_m \sum_n D_{mn}^{(o)-\lambda}[(ik,mn) - 1/2(im,kn)] \quad (5\text{-}3)$$

The constrained conditions in the RHF$^{\pi}$-f and RHF$^{\pi}$-m ensure all the $D_{mn}^{(\pi)-\sigma}$ and $D_{mn}^{(o)-\sigma}$ ($m \neq n$) are equal to zero except those between two pairs of the single occupied FMOs. In these cases, the effect of the σ-electron delocalization on the π system has been eliminated as far as possible.

In order to get deeper insight into the conjugation effect on the original energies $E_p^{(o)-\pi}$, the energy effect $\Delta E_{\pi}^{(\pi)}(\theta)$ including its components $\Delta E_{pq}^{(\pi)-\pi}(\theta)$ and $\Delta E_p^{(\pi)-\pi}(\theta)$ were calculated (Tables 3 and 4). In accord with the classic viewpoint, the conjugation energy $\Delta E_{ab+bc}^{(\pi)-\pi}(\theta)$ is most stabilizing at the coplanar geometry, and weakens with the rotation of fragment C about the C_1-N_7 bond. The absolute value (|−1.1369|hartree) of $\Delta E_{ab+bc}^{(\pi)-\pi}$ in the coplanar geometry is greatest of all the rotational geometries listed in Table 3, and its minimum value, about |−0.000 99|hartree, occurs in the vertical geometry with $\alpha = \theta = 90°$. However, as shown by the data in Tables 3 and 4, the conjugation reduces, without exception, the original π energy $E_p^{(o)-\pi}$ of each of fragments, and, moreover, the energy

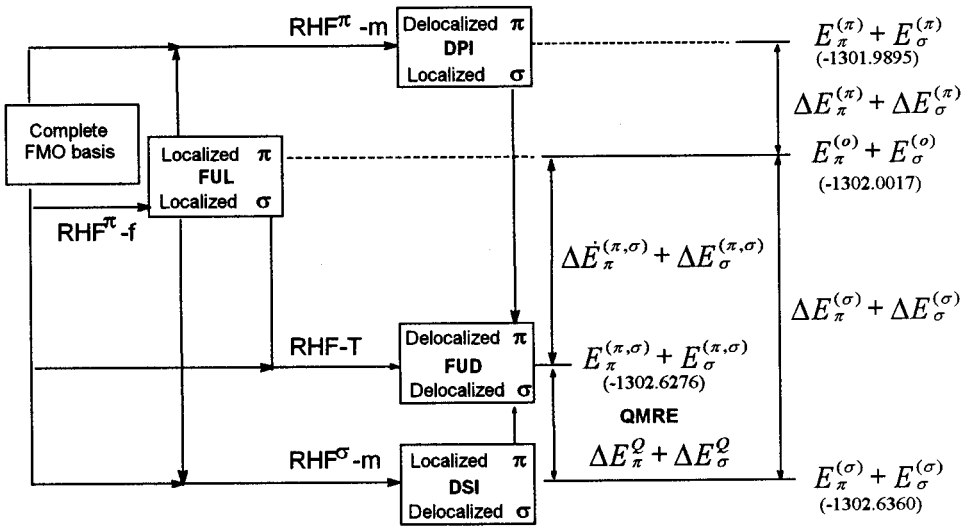

Figure 5. The thermodynamic cycle for the orbital interactions and the definitions of the various energy differences. The numbers in parentheses are the values (hartrees) of the total electronic energies in four hypothetical states (FUL, DPI, DSI, and FUD) of the copolanar geometry of **1h**.

TABLE 3: Energy Gain $\Delta E_{pq}^{(\pi)-\pi}$, Energy Losses $\Delta E_{p}^{(\pi)-\pi}$, Total π and σ Interaction Energies $\Delta E_{\pi}^{(\pi)}$ and $\Delta E_{\sigma}^{(\pi)}$, and Total Electronic Energies $E_{\pi}^{(\pi)}$ and $E_{\sigma}^{(\pi)}$ in the DPI State of 1h, and Their Changes with the Rotation of Fragment C (Energy in Hartrees)

angle (deg)										
θ	α	$\Delta E_{ab}^{(\pi)-\pi}$	$\Delta E_{bc}^{(\pi)-\pi}$	$\Delta E_{a}^{(\pi)-\pi}$	$\Delta E_{b}^{(\pi)-\pi}$	$\Delta E_{c}^{(\pi)-\pi}$	$\Delta E_{\pi}^{(\pi)}$	$\Delta E_{\sigma}^{(\pi)}$	$E_{\pi}^{(\pi)}$	$E_{\sigma}^{(\pi)}$
					Model II of Optimizing					
0	0	−0.544 29	−0.592 56	0.550 15	0.433 80	0.242 19	0.088 67	−0.076 47	−134.7154	−1167.2741
10	0	−0.542 14	−0.574 64	0.549 37	0.420 35	0.234 03	0.086 63	−0.074 58	−134.7285	−1167.3118
30	0	−0.528 31	−0.445 13	0.544 42	0.321 17	0.179 43	0.071 33	−0.060 44	−134.8300	−1167.6070
50	0	−0.504 27	−0.248 88	0.532 71	0.158 33	0.107 83	0.045 58	−0.036 63	−134.9147	−1167.6222
90	0	−0.474 11	−0.000 68	0.516 63	−0.054 51	0.023 01	0.010 34	−0.003 35	−134.9125	−1167.0489
90	90	−0.000 30	−0.000 69	0.000 34	0.000 49	0.000 20	0.000 05	−0.000 08	−135.0351	−1167.1675
					Model I of Optimizing					
0		−0.541 44	−0.592 20	0.547 48	0.432 71	0.242 36	0.088 54	−0.076 36	−134.7147	−1167.2647
10		−0.536 62	−0.574 43	0.544 06	0.418 05	0.235 70	0.086 40	−0.074 40	−134.7296	−1167.3036
30		−0.526 65	−0.454 66	0.542 47	0.322 35	0.188 71	0.071 89	−0.061 03	−134.8072	−1167.4844
50		−0.505 65	−0.271 93	0.532 61	0.172 14	0.121 31	0.048 31	−0.039 10	−134.8507	−1167.3113
90		−0.473 32	−0.002 91	0.516 33	−0.056 07	0.025 67	0.009 68	−0.002 73	−134.8104	−1166.4864

gain $\Delta E_{ab+bc+ca}^{(\pi)-\pi}(\theta)$ is insufficient to compensate for the total energy loss $\Delta E_{a+b+c}^{(\pi)-\pi}(\theta)$. The total π energy effect $\Delta E_{\pi}^{(\pi)}(\theta)$ is destabilizing. The $\Delta E_{\pi}^{(\pi)}(0°)$ of **1h** is large up to 55.64 kcal/mol. At the vertical geometry, there should be no π interactions between fragments except the long distance interaction between fragments A and C. The calculation results are $\Delta E_{ab+bc}^{(\pi)-\pi} = -0.62$ kcal/mol and $\Delta E_{\pi}^{(\pi)} = 0.031$ kcal/mol (Table 3).

As shown by the data of $\Delta E_{\sigma}^{(\pi)}(\theta)$ in Tables 3 and 4, the σ framework is stabilized owing to the $\sigma-\pi$ space interactions, while the π system itself is destabilized due to the π-electron interactions between fragments. However, this energy gain $\Delta E_{\sigma}^{(\pi)}(\theta)$ is still insufficient to compensate for the π energy loss $\Delta E_{\pi}^{(\pi)}(\theta)$. The total energy effect $\Delta E_{\pi}^{(\pi)}(\theta) + \Delta E_{\sigma}^{(\pi)}(\theta)$ is destabilizing. At the coplanar geometry of **1h**, for example, its value (7.66 kcal/mol) is greatest, and the total electronic energy (−1301.9895 hartrees) in the DPI state is the highest of four hypothetical electronic states (see Figure 5). It might be a reason why the symmetrization of the phenyl ring in **1h-VER** is better than that of **1h-R0** (Figure 3).

Destabilization of the π-System in the DPI State Is Due to π-Electron Delocalization. Electron delocalization is an important concept in modern organic chemistry. One problem is that "delocalization" is not directly measurable and there is no single definition underlying the use of this concept throughout chemistry.[23] As shown by Figure 6, the charge transfer (CT) mixes the occupied FMO of one fragment with the vacant FMO of the other and vice versa, and one of two exchange (EX) energies is associated with the interaction between the occupied FMOs. According to the Morokuma definitions,[15] these two interactions cause π-electron delocalization between fragments. Based on the PMO expression for two-electron interaction energy,[24] the CT energy Σ_{ov}^{pq} (Figure 6) can be defined as the energy gain of fragment P, and it is associated with the interaction which causes the delocalization of the π-electrons from P to Q. Comparison of the values of the Σ_{p}^{2} and the net π-electron charge $D_{\rho}^{(\pi)}$ (Table 5) and inspection of their signs indicate that the quantity Σ_{p}^{2}, as defined by eqs (6-1)−(6-3), can be used to measure, indirectly, the net charge transfer.

$$\Sigma_{a}^{2} = \Sigma_{ov}^{ba} - \Sigma_{ov}^{ab} \tag{6-1}$$

$$\Sigma_{c}^{2} = \Sigma_{ov}^{bc} - \Sigma_{ov}^{cb} \tag{6-3}$$

$$\Sigma_{b}^{2} = -(\Sigma_{a}^{2} + \Sigma_{c}^{2}) \tag{6-2}$$

whether fragment P is a +M or −M group depends upon the sign of Σ_{p}^{2}. The signs of the $D_{a}^{(\pi)}$ and Σ_{a}^{2} both are positive without exception; fragment A is +M group as far as two-electron interaction is concerned. On the other hand, it is difficult to determine the contributions made by each of two

TABLE 4: Energy Gain $\Delta E_{ab+bc}^{(\pi)-\pi}$, Energy Losses $\Delta E_{p}^{(\pi)-\pi}$, CT Energy Σ_{ov}^{cb}, Total π and σ Interaction Energies $\Delta E_{\pi}^{(\pi)}$ and $\Delta E_{\sigma}^{(\pi)}$, Total Electronic Energies $E_{\pi}^{(\pi)}$ and $E_{\sigma}^{(\pi)}$ in the DPI State of Stilbene-like Species, and the Changes with the Rotation of Fragment C (Energy in Hartrees)

angle (deg)											
θ	α	$\Delta E_{ab+bc}^{(\pi)-\pi}$	$\Delta E_{a}^{(\pi)-\pi}$	$\Delta E_{b}^{(\pi)-\pi}$	$\Delta E_{c}^{(\pi)-\pi}$	Σ_{ov}^{cb}[a]	$\Delta E_{\pi}^{(\pi)}$	$\Delta E_{\sigma}^{(\pi)}$	$E_{\pi}^{(\pi)}$	$E_{\sigma}^{(\pi)}$	model
					Compound **1a**						
0	0	−1.156 54	0.392 98	0.463 76	0.391 81	−0.469 82	0.091 47	−0.077 24	−132.1603	−1131.6589	II
5	5	−1.146 70	0.390 12	0.458 76	0.389 18	−0.466 52	0.090 83	−0.076 71	−132.1687	−1131.6866	I
20	20	−1.010 44	0.351 21	0.390 41	0.350 51	−0.419 28	0.081 69	−0.068 87	−132.2658	−1131.9565	I
					Compound **1j**						
0	0	−1.086 10	0.370 63	0.443 10	0.359 74	−0.424 78	0.087 06	−0.074 61	−134.5834	−1166.7678	II
5		−1.081 24	0.370 70	0.440 27	0.357 19	−0.421 71	0.086 61	−0.074 22	−134.5856	−1166.7696	I
20		−1.015 04	0.373 17	0.403 28	0.319 36	−0.376 72	0.080 48	−0.068 61	−134.6308	−1166.9018	I
					Compound **1h**						
0	0	−1.136 85	0.550 15	0.433 80	0.242 19	−0.401 70	0.088 68	−0.076 62	−134.7154	−1167.2741	II
5		−1.129 79	0.548 20	0.429 52	0.240 48	−0.398 80	0.088 06	−0.075 98	−134.7182	−1167.2761	I
					Compound **1f**						
0	0	−1.187 51	0.436 23	0.604 73	0.232 78	−0.399 47	0.085 97	−0.075 19	−193.9805	−1588.3054	II
5		−1.182 36	0.435 96	0.601 38	0.230 87	−0.396 55	0.085 61	−0.074 82	−193.9824	−1588.3087	I
20		−1.115 67	0.435 65	0.554 78	0.205 94	−0.356 36	0.080 50	−0.069 99	−194.0056	−1588.3379	I
					Compound **1e**						
0	0	−1.178 91	0.538 06	0.547 58	0.180 87	−0.382 01	0.087 32	−0.076 22	−168.3976	−1754.1825	II
5		−1.171 11	0.534 28	0.544 25	0.179 57	−0.378 47	0.086 74	−0.075 76	−168.3997	−1754.1976	I
20		−1.104 93	0.530 53	0.495 18	0.160 74	−0.340 69	0.081 28	−0.070 68	−168.4250	−1754.2161	I
					Compound **1g**[b]						
0	0	−1.236 37	0.823 43	0.431 83	0.056 22	−0.345 69	0.074 71	−0.064 45	−158.8848	−1292.3778	II
5		−1.231 94	0.822 73	0.427 97	0.055 95	−0.343 45	0.074 31	−0.064 10	−158.8863	−1292.3785	I
20		−1.163 73	0.812 81	0.369 94	0.049 61	−0.308 33	0.068 28	−0.058 35	−158.9106	−1292.4070	I
					Compound **1i**						
0	0	−1.175 75	0.493 97	0.716 34	0.048 37	−0.333 22	0.082 75	−0.072 86	−195.1525	−1605.7806	II
5		−1.170 04	0.492 91	0.711 34	0.048 27	−0.330 88	0.082 29	−0.072 37	−195.1545	−1605.7823	I
20		−1.105 63	0.488 24	0.649 97	0.044 36	−0.297 89	0.076 76	−0.067 37	−195.1867	−1605.8563	I

[a] The energy effect Σ_{ov}^{cb} will be defined and used in the next section. [b] -N(Me)$_2$ group in **1g** has been replaced with a planar -NH$_2$.

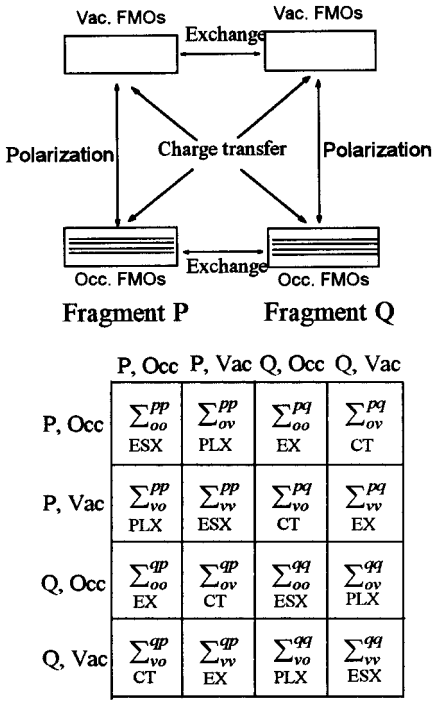

Figure 6. Morokuma's definitions of the FMO interactions between fragments P and Q (P, Q = A, B, C).

fragments to the EX energy Σ_{oo}^{pq}. Referring to the method for calculating the gross AO's charge,[25] the EX energy might be able to be divided evenly into two parts $\Sigma_{oo}^{pq} = (1/2)\Sigma_{oo}^{pq} + (1/2)\Sigma_{oo}^{qp}$ (Table 5); still we cannot say which fragment is a −M group as far as the four-electron interaction is concerned.

A comparison of the data in Table 5 with the corresponding $\Delta E_{p}^{(\pi)-\pi}(\theta)$ in Table 3 shows that the energy losses $\Delta E_{b}^{(\pi)-\pi}(\theta)$ and $\Delta E_{c}^{(\pi)-\pi}(\theta)$ become larger while the absolute values of the $\Sigma_{ov}^{bc}(\theta) + \Sigma_{ov}^{ba}(\theta)$ and the $\Sigma_{ov}^{cb}(\theta)$ increase with the geometry of **1h** getting flatter. At the coplanar geometry, for example, the $\Sigma_{ov}^{bc}(0°) + \Sigma_{ov}^{ba}(0°)$ (−0.874 72 hartree) and $\Sigma_{ov}^{cb}(0°)$ (−0.401 87) are most stabilizing, and the corresponding $\Delta E_{b}^{(\pi)-\pi}(0°)$ (0.242 36) and $\Delta E_{c}^{(\pi)-\pi}(0°)$ (0.432 71) both are most destabilizing. In Table 4, there are seven sets of the data listed in increasing order of the value of $\Sigma_{ov}^{cb}(0°)$ in each of seven compounds. Table 4 shows further that from compound **1a** to **1i**, the value of the $\Delta E_{c}^{(\pi)-\pi}(0°)$ decreases as the absolute value of the $\Sigma_{ov}^{cb}(0°)$ decreases. In molecule **1a**, for example, the absolute value (|−0.4698|hartree) of the $\Sigma_{ov}^{cb}(0°)$ and the value (0.3918 hartree) of the corresponding $\Delta E_{c}^{(\pi)-\pi}(0°)$ both are greatest, and the smallest values (|−0.3332| and 0.0484 hartree) of these two energies both occur in **1i**. This comparison also indicates that in a given geometry with the $\theta \neq 50°$, a larger energy loss $\Delta E_{p}^{(\pi)-\pi}(\theta)$ corresponds to a larger value of the $\Sigma_{p}^{2}(\theta)$. In the $\theta = 0°$ geometry (Model I) of **1h**, for example, the value of the $\Sigma_{p}^{2}(0°)$ decreases in the sequence: $\Sigma_{a}^{2}(0°) = 0.135\ 70$ hartree > $\Sigma_{b}^{2}(0°) = -0.017\ 46$ > $\Sigma_{c}^{2}(0°) = -0.118\ 24$, and the value of the corresponding $\Delta E_{p}^{(\pi)-\pi}(0°)$ decreases in the same sequence: $\Delta E_{a}^{(\pi)-\pi}(0°) = 0.547\ 48$ hartree > $\Delta E_{b}^{(\pi)-\pi}(0°) = 0.432\ 71$ > $\Delta E_{c}^{(\pi)-\pi}(0°) = 0.242\ 36$.

Every π system with $\Sigma_{pq}^{ov}(\theta) < 0.0$ is destabilized (except $\Delta E_{b}^{(\pi)-\pi}(90°)$), and which one is most destabilized depends upon their values of $\Sigma_{p}^{2}(\theta)$.

TABLE 5: CT Energies Σ_{ov}^{pq}, Net CT Energies Σ_{p}^{2}, EX Energies Σ_{oo}^{pq} Occurring in Five Typical Geometries (Model I) of 1h, and the Net π-Electron Charge $D_{p}^{(\pi)}$ on Each of Three Fragments (Energy in Hartrees)

	$\theta = 0°$	$\theta = 10°$	$\theta = 30°$	$\theta = 50°$	$\theta = 90°$
			Fragment A		
Σ_{ov}^{ab}	−0.490 32	−0.488 31	−0.495 35	−0.500 18	−0.503 93
Σ_{a}^{2}	0.135 70	0.136 46	0.147 20	0.160 95	0.180 64
$0.5\Sigma_{oo}^{ab}$	0.162 41	0.162 10	0.166 66	0.171 87	0.177 42
$D_{a}^{(\pi)}$	0.026 22	0.026 14	0.026 60	0.026 81	0.027 03
			Fragment B		
$\Sigma_{ov}^{ba} + \Sigma_{ov}^{bc}$	−0.874 72	−0.856 96	−0.749 94	−0.580 52	−0.325 57
Σ_{b}^{2}	−0.017 46	−0.021 43	−0.052 91	−0.103 12	−0.180 62
$0.5(\Sigma_{oo}^{ba} + \Sigma_{oo}^{bc})$	0.350 36	0.345 03	0.313 19	0.260 89	0.178 05
$D_{b}^{(\pi)}$	−0.013 49	−0.013 78	−0.016 43	−0.020 58	−0.027 12
			Fragment C		
Σ_{ov}^{cb}	−0.401 87	−0.390 08	−0.307 50	−0.183 46	−0.002 27
Σ_{c}^{2}	−0.118 24	−0.115 03	−0.094 29	−0.057 84	0.000 60
$0.5\Sigma_{oo}^{cb}$	0.187 95	0.182 93	0.146 53	0.089 02	0.000 63
$D_{c}^{(\pi)}$	−0.012 73	−0.012 36	−0.010 17	−0.006 23	0.000 09

TABLE 6: QMRE of 1h, Its π and σ Components ΔE_{π}^{Q} and ΔE_{σ}^{Q}, Total π and σ Electronic Energies $E_{\pi}^{(\pi,\sigma)}$ and $E_{\sigma}^{(\pi,\sigma)}$ in the FUD State, and Their Changes with the Rotation of Fragment C (Energy in Hartrees)

angle (deg)						
θ	α	QMRE	ΔE_{π}^{Q}	ΔE_{σ}^{Q}	$E_{\pi}^{(\pi,\sigma)}$	$E_{\sigma}^{(\pi,\sigma)}$
0	0	0.008 44	−0.083 13	0.091 57	−134.661 80	−1167.965 79
350	0	0.008 23	−0.084 98	0.093 21	−134.674 40	−1168.006 13
330	0	0.006 94	−0.099 35	0.106 29	−134.772 34	−1168.319 01
310	0	0.004 89	−0.125 24	0.130 13	−134.854 25[a]	−1168.357 51[a]
270	0	0.002 87	−0.161 32	0.164 19	−134.851 51	−1167.805 82

[a] Maximal absolute values.

TABLE 7: QMRE of Stilbene-like Species, and Their π and σ Components ΔE_{π}^{Q} and ΔE_{σ}^{Q} at the Planar Geometry (Hartrees)

compds	QMRE	ΔE_{π}^{Q}	ΔE_{σ}^{Q}
1a	0.014 10	0.009 27	0.004 83
1j	0.009 41	−0.065 70	0.075 11
1h	0.008 44	−0.083 13	0.091 57
1e	0.007 77	−0.049 56	0.057 37
1f	0.007 70	−0.055 59	0.063 29
1i	0.006 84	−0.041 25	0.048 09
1g	0.006 30	−0.083 24	0.089 54

The Quantum Mechanical Resonance Energy (QMRE) of Stilbene-like Species Is Destabilizing. According to the original definition,[26] the QMRE of a delocalized system in a given geometry of benzene is the difference between the energy of the true ground state and the energy of a single Kekule structure. In this work, it is defined as the difference in the electronic energy between the FUD and DSI states. As shown by Tables 6 and 7, the QMRE of each of STB-type **1** is destabilizing. The QMRE (0.008 44 hartree) of **1h**, for example, is most destabilizing at its planar geometry (Table 6), and its value monotonically decreases with the rotation of fragment C. A comparison of the data in Table 7 with those in Table 4 and Table 1 shows that of all molecules listed in the tables, a larger QMRE (>0.008 hartree), such as those 0.0141, 0.0094, and 0.0084 hartree, respectively, in **1a**, **1j**, and **1h** (Table 7) corresponds generally to a larger $\Sigma_{ov}^{cb}(0°)$ and to a larger sum ($\phi + \alpha > 35°$) (Table 1).

It is known that benzene is strongly stabilized by the QMRE.[27] In order to make a comparison between the QMREs of benzene and molecules of type **1**, and to understand the role of the QMRE with regard to molecular geometry and chemical reactivity, the distortion of the benzene geometry, denoted as d_{SH}, is considered in this work, and the various energies occurring in six typical d_{SH} geometries were calculated (Table 8). The d_{SH} distortion was previously investigated by Shaik and Hiberty.[28] The geometries $d_{SH} \neq 0.0$ Å arise from variations in alternating CC bond lengths within the constraint that the contribution of the nuclear repulsion to the total energy remains constant, equal to that of the $d_{SH} = 0.0$ Å geometry. The $d_{SH} = 0.1644$ Å geometry resembles an idealized cyclohexatriene structure of alternating single and double CC bond lengths R'_{cc} and R_{cc} (see Table 8). In our PMO calculation, a distorted benzene molecule was dissected into three ethylenic fragments A, B, and C. In each of three fragments, the length of the CC double bond was equal to that of the shorter R_{cc} in the composite system. Table 8 shows that the QMRE is most stabilizing at the $d_{SH} = 0.0$ Å geometry and monotonically weakens as the carbon framework is increasingly distorted away from the $d_{SH} = 0.0$ Å. At the $d_{SH} = 0.0$ Å geometry, for example, the QMRE is −43.28 kcal/mol, and it is the average of the spectroscopy value[29a] (−50 kcal/mol) and that (−36 kcal/mol)[29b] suggested by thermochemical measures. However, the detail energy partition shows that the QMRE is a sum of two components $\Delta E_{\sigma}^{Q} = E_{\sigma}^{(\pi,\sigma)} - E_{\sigma}^{(\sigma)}$ and $\Delta E_{\pi}^{Q} = E_{\pi}^{(\pi,\sigma)} - E_{\pi}^{(\sigma)}$. Whether the QMRE is stabilizing or destabilizing depends upon the response, expressed in terms of the $\Delta E_{\sigma}^{Q}(d_{SH})$ and $\Delta E_{\sigma}^{Q}(\theta)$, respectively, of the σ frameworks to the delocalization of the π-electrons. In the case of STB-type **1**, $\Delta E_{\sigma}^{Q}(\theta)$ is always destabilizing and its value is slightly larger than the absolute value of the corresponding $\Delta E_{\pi}^{Q}(\theta)$ which is generally stabilizing except for that in **1a**. Conversely, the $\Delta E_{\sigma}^{Q}(d_{SH})$, as shown by the data in Table 8, is always stabilizing, and the $\Delta E_{\pi}^{Q}(d_{SH})$ is generally destabilizing except that in the $d_{SH} = 0.0$ Å geometry of benzene. Particularly, the absolute value (|−0.0533|hartree) of the $\Delta E_{\sigma}^{Q}(d_{SH} = 0.0)$ is about three time larger than that (|−0.0177|hartree) of the $\Delta E_{\pi}^{Q}(0.0)$. Therefore, it is the σ

TABLE 8: QMRE (kcal/mol) of Benzene, Its Components ΔE_π^Q and ΔE_σ^Q, Electronic Energies $E_\pi^{(\sigma)}$ and $E_\sigma^{(\sigma)}$ in the DSI State, Those $E_\pi^{(\pi,\sigma)}$ and $E_\sigma^{(\pi,\sigma)}$ in the FUD State, and Their Changes along the d_{SH} Distortion (Energy in Hartrees except for QMRE)

d_{SH} (Å)	0.0	0.0403	0.0811	0.1224	0.1644	0.2070
R_{cc} (short)	1.40 Å	1.38	1.36	1.34	1.32	1.30
R_{cc} (long)	1.40 Å	1.4203	1.4411	1.4624	1.4844	1.5070
QMRE	−43.281 875	−31.083 080	−20.865 963	−12.554 593	−5.868 474	−0.626 882
ΔE_π^Q	−0.017 645	0.001 388	0.015 810	0.026 050	0.0328 05	0.036 767
ΔE_σ^Q	−0.051 329	−0.050 922	−0.049 062	−0.046 057	−0.042 157	−0.037 766
$E_\pi^{(\sigma)}$	−39.744 438	−39.765 388	−39.786 453	−39.807 735	−39.827 721	−39.847 374
$E_\sigma^{(\sigma)}$	−391.040 527	−391.036 011	−391.029 022	−391.020 599	−391.001 709	−390.978 485
$E_\pi^{(\pi,\sigma)}$	−39.762 085	−39.764 000	−39.770 645	−39.781 689	−39.794 918	−39.810 608
$E_\sigma^{(\pi,\sigma)}$	−391.091 858	−391.086 914	−391.078 094	−391.066 681	−391.043 884	−391.016 266

TABLE 9: Occupied π MOs and Energy Changes along the d_{SH} Distortion (Energy in Hartrees)[a]

d_{SH} (Å)	0.0	0.0403	0.0811	0.1224	0.1644	0.2070
			DSI State			
21st (HOMO)	−0.331 63	−0.335 56	−0.339 77	−0.344 28	−0.349 04	−0.354 10
			FUD State			
21st (HOMO)	−0.278 24	−0.279 02	−0.281 37	−0.285 13	−0.290 10	−0.296 09
17th	−0.453 21	−0.453 21	−0.453 27	−0.453 44	−0.453 75	−0.454 29

[a] In the DSI state, three occupied π MOs, 21st, 20th, and 19th, are degenerate. There are doubly degenerate levels, 21st and 20th, in the FUD state.

TABLE 10: Total Electronic Energy E_e, Nuclear Repulsion E_υ, Total Molecular Energy E^T, Potential Energies $RE_\pi^{(\sigma)}$ and $RE_\sigma^{(\sigma)}$, and Electronic Energies $E_\pi^{(\sigma)}$ and $E_\sigma^{(\sigma)}$ in the DSI State of Five Typical Geometries of 1h (Energy in Hartrees)

θ (deg)	$RE_\pi^{(\pi)}$	$RE_\sigma^{(\sigma)}$	$E_\pi^{(\sigma)}$	$E_\sigma^{(\sigma)}$	E_e	RE_e	E_υ	E^T
				Model I of Optimizing				
0[a]	0.0000	0.0000	−134.5778	−1168.0484	−1302.6175	0.0000	740.5334	−562.0842
350	−0.0149	−0.0434	−134.5902	−1168.0918	−1302.6718	−0.0543	740.5874	−562.0844
330	−0.0827	−0.2531	−134.6510	−1168.3015	−1302.9333	−0.3158	740.8477	−562.0855
310	−0.1360	−0.1243	−134.6682	−1168.1727	−1302.8076	−0.1901	740.7220	−562.0856
270	−0.0957	0.6393	−134.5876	−1167.4091	−1301.9436	0.6739	739.8610	−562.0826

[a] The referential geometry for the calculations of the potential energies. The energies E_υ, E_e, and E^T were obtained from full SCF computation at the STO-3G level.

framework for the d_{SH} = 0.0 Å geometry to be strongly stabilized by the QMRE. Benzene is σ aromatic.[30] On the other hand, the π potential energy $RE_\pi^{(\pi,\sigma)}(0.0) = E_\pi^{(\pi,\sigma)}(0.0) - E_\pi^{(\pi,\sigma)}(0.1644)$ is large, up to 20.6 kcal/mol (Table 8), revealing that the π-system of benzene is destabilized, and it prefers a distorted geometry.[31]

In the DSI state of benzene, the differences $dE_\sigma^{(\sigma)}(d_{SH}) = E_\sigma^{(\sigma)}(d_{SH}) - E_\sigma^{(\sigma)}(d_{SH}^o) < 0.0$, $dE_\pi^{(\sigma)}(d_{SH}) = E_\pi^{(\sigma)}(d_{SH}) - E_\pi^{(\sigma)}(d^o{}_{SH}) > 0.0$ when $d_{SH} < d_{SH}^o$, and the absolute value of the $dE_\sigma^{(\sigma)}(d_{SH})$ is less than that of the $dE_\pi^{(\sigma)}(d_{SH})$. The $dE_\sigma^{(\sigma)}(d_{SH})$ between the d_{SH} = 0.0 and 0.1644 Å geometries is, for example, −24.359 kcal/mol, and the corresponding $dE_\pi^{(\sigma)}(d_{SH})$ is large up to 52.261 kcal/mol. The σ-framework in the DSI state only possesses a distortive tendency. It is the π delocalization to make this tendency become an effective driving force, expressed in terms of the $dE_\sigma^{(\pi,\sigma)}(d_{SH}) = [E_\sigma^{(\pi,\sigma)}(d_{SH}) - E_\sigma^{(\pi,\sigma)}(d_{SH}^o)]$ whose absolute value is now larger than that of the $dE_\pi^{(\pi,\sigma)}(d_{SH}) = E_\pi^{(\pi,\sigma)}(d_{SH}) - E_\pi^{(\pi,\sigma)}(d_{SH}^o)$, for distorting the $d_{SH} \neq 0.0$ Å toward the symmetrical geometry.[31] The $dE_\sigma^{(\pi,\sigma)}(d_{SH} = 0.0)$ between the d_{SH} = 0.0 and 0.1644 Å geometries is, for example, −30.104 kcal/mol, and the corresponding $dE_\pi^{(\pi,\sigma)}(0.0)$ = 20.603 kcal/mol.

Table 9 shows further that in a given d_{SH} geometry, the energy of the highest occupied MO (HOMO) of the π type in the FUD state is always higher than that in the DSI state. Along the d_{SH} distortion, the energy, about −0.278 24 hartree, of the HOMO is highest at the d_{SH} = 0.0 Å geometry. This energy character, together with those indicated by the $E_\pi^{(\pi,\sigma)}(d_{SH})$ in Table 8 and the $E_\pi^{(\pi,\sigma)}(\theta)$ in Table 6, is in accordance with the chemical feature that the π systems of benzene and STB-type **1** both are reactive toward electronphilic attack. However, the high stability of benzene due to the $\Delta E_\sigma^Q(0.0) < 0.0$ (−32.21 kcal/mol) is getting weaker while its π-system is increasingly localized under the electrophile attacking. In the transition state, the σ-framework of benzene is reluctant to undergo addition reaction and has to opt for "aromatic" substitution instead in order to maintain its original σ-aromaticity. On the other hand, STB-type **1** are willing to undergo addition reaction owing to their $\Delta E_\sigma^Q(\theta) > 0.0$. During the period of preparing **1i**, we found that the -CH═N- double bond is very unstable in its alcohol solution; the addition product is 2-ethoxyl-2-(4-nitrophenyl)-*N*-(2-pyrimidyl)ethylamine.

***σ* Interaction Is a Main Driving Force for Out-of-Plane Twist.** The electronic energy of the DSI state is the lowest of four hypothetical states. In this state, all the elements, such as $F_{ij}^{(\sigma)-\pi}$, $H_{ij}^{(\sigma)-\pi}$, and $D_{ij}^{(\sigma)-\pi}$ ($i \neq j$) corresponding to those in eqs (3-1)−(3-2), are equal to zero. Therefore, the potential energy, denoted as $RE_\sigma^{(\sigma)}(\theta) = E_\sigma^{(\sigma)}(\theta) - E_\sigma^{(\sigma)}(0°)$, is useful for analyzing the molecular conformation. In the region of the θ from 0 to about 40°, the absolute values of the various energies in **1h**, such as the $E_\sigma^{(\sigma)}(\theta)$, $E_e(\theta)$ (Table 10), and $E_\pi^{(\pi)}(\theta)$ (Table 3), increase concurrently as the nuclear repulsion E_υ (Table 10) becomes larger. In a given conformer, the absolute value of $RE_\sigma^{(\sigma)}(\theta)$ is generally three times larger than that of the $RE_\pi^{(\pi)}(\theta)$, and it is very close to that of the $RE_e(\theta)$. The

TABLE 11: Total σ-Electronic Energy $E_\sigma^{(\sigma)}$ in the DSI States, Net σ-Electron Charge $D_c^{(\sigma)}$ and the Ratio, $de/d\upsilon$, of the $dE_\sigma^{(\sigma)}$ to dE_υ (Energy in Hartrees)

θ (deg)	$E_\sigma^{(\sigma)}$	$D_c^{(\sigma)}$	$de/d\upsilon$
	1h		
0	−1168.0484	0.109 37	
5	−1168.0606	0.109 51	−0.82
	1i		
0	−1606.5901	0.091 59	
5	−1606.5965	0.091 74	−0.80
	1g		
0	−1293.1949	0.101 49	
5	−1293.1985	0.101 58	−0.78
	1j		
0	−1167.5517	0.125 02	
5	−1167.5543	0.125 15	−0.82
	1f		
0	−1589.1171	0.112 83	
5	−1589.1206	0.112 95	−0.74
	1e		
0	−1754.9791	0.109 45	
5	−1754.9830	0.109 56	−0.69

$RE_\sigma^{(\sigma)}$ plays a predominant role in determining the preferential geometry of **1h**.

In flexible molecules such as STB-type **1**, it is difficult to determine which pair of the atoms makes the greatest contribution to the driving force. According to the definition $E_\upsilon = \Sigma_i\Sigma_j(e_ie_j/r_{ij})$, E_υ can be, indirectly, used to characterize the interaction distance between fragments, and the quantity $de/d\upsilon$ in eq 7 can be defined as a generalized driving force for the out-of-plane twist.

$$de/d\upsilon = [E_\sigma^{(\sigma)}(5°) - E_\sigma^{(\sigma)}(0°)]/[E_\upsilon(5°) - E_\upsilon(0°)] \quad (7)$$

Comparison of the values of $de/d\upsilon$ in Table 11 and those of the angle ϕ in Table 1 shows that a larger absolute value (>0.80) of the $de/d\upsilon$ corresponds to a larger twist angles ϕ (>30°). The calculations for the net σ electronic charge $D_c^{(\sigma)}(\theta)$ of fragment C (Table 11) show that, in the three typical molecules, the values of the $dD_c^{(\sigma)} = D_c^{(\sigma)}(5°) - D_c^{(\sigma)}(0°)$ are in the sequence: 1.5×10^{-4} (**1i** with a -NO_2 group and two ring-nitrogen atoms) $>1.4 \times 10^{-4}$ (**1h** with a ring-nitrogen atom on fragment C) $>1.3 \times 10^{-4}$ (**1j** with a ring-nitrogen atom on fragment A), and their respective values of the angle ϕ are 50 (**1i**) > 38 (**1h**) > 35° (**1j**). It seems that the electron-withdrawing (−I) groups and the ring-nitrogen atoms have an obvious influence upon the twist angle.

Summary

We have been successful in separating σ from π FMOs based on our new procedure. Besides the well-known resonance interaction between fragments, the σ-electron interaction, arising from the effect of the π-electron delocalization on the $\sigma-\pi$ space interactions, is also stabilization. However, the delocalization of the π-electrons in the DPI state not only reduces the original π energies in fragments, but also the energy gains are insufficient to compensate for the energy loss. The π-electron delocalization in the DPI state is found to be destabilization. As a result, the DPI state is most destabilized at a coplanar geometry, and, in a given geometry, its electronic energy is highest of four hypothetical states. The characteristic of the QMRE depends upon the response of the σ framework to the π delocalization. In the case of stilbene-like species, the QMRE is destabilizing. On the other hand, the QMRE of benzene is stabilizing. However, it is the σ framework, rather than the π system itself, which is strongly stabilized by the QMRE, revealing that benzene is σ aromatic.

Contrary to the viewpoints in the literature, the driving forces for the out-of-plane twist of stilbene-like species are due to the σ orbital interaction and the QMRE. It seems that the electron-withdrawing (−I) groups on the aromatic ring and the ring-nitrogen atoms, has an obvious influence on the twist angle.

Experimental Section

General Methods. All starting materials were obtained commercially as reagent grade. Melting points were determined on a Nagoya apparatus and are uncollected. ^{1}H NMR spectra were recorded on a Varian Unity 200 NMR spectrometer. Crystal structures of molecules were determined by a Nicolet R3WE X-ray diffractometer. The crystal data of each of the following eight compounds are listed in Table 12.

***N*-(4-Chlorophenyl)methylene-2-pyridineamine (1e)** was prepared from 4-chlorobenzaldehyde and 2-pyridineamine:[32] mp 96−99 °C; ^{1}H NMR ($CDCl_3$) 9.12 (s, 1H), 8.56 (d, 1H), 7.18−7.92 (m, 7H).

***N*-(4-Nitrophenyl)methylene-2-pyridineamine (1f)** was prepared from 4-nitrobenzaldehyde and *N*-(triphenylphosphoranylidene)-2-pyridineamine:[32] mp 147−148 °C; ^{1}H NMR ($CDCl_3$) 9.27 (s, 1H), 8.58 (d, 1H), 8.38−7.25 (m, 7H).

***N*-(4-*N*,*N*-Dimethylaminophenyl)methylene-2-pyridineamine (1g)** was prepared from 4-*N*,*N*-dimethylbenzaldehyde and 2-pyridineamine:[32] mp 123−124 °C; ^{1}H NMR ($CDCl_3$) 9.1 (s, 1H), 8.50 (d, 1H), 7.9−6.8 (m, 7H), 3.2 (s, 6H).

***N*-(4-Nitrophenyl)methylene-2-pyrimidineamine (1i)** was prepared from 4-nitrobenzaldehyde and *N*-(triphenylphospho-

TABLE 12: Crystal Data of Four Stilbene-like Molecules 1 and Four Ketenimine Derivatives 2[a]

	1e	**1f**	**1g**	**1i**	**2a**	**2b**	**2c**	**2d**
formula	$C_{12}H_9ClN_2$	$C_{12}H_9N_3O_2$	$C_{14}H_{15}N_3$	$C_{11}H_8N_4O_2$	$C_{20}H_{15}N$	$C_{20}H_{14}N_2O_2$	$C_{22}H_{18}N_2O_4$	$C_{22}H_{20}N_2$
fw	216.66	227.220	225.290	228.210	269.00	314.330	374.380	312.400
color	colorless	yellow	yellow	yellow	yellow	red		yellow
a	6.509	7.096	11.923	6.015	20.594	7.972	13.439	9.919
b	8.005	28.754	17.914	13.393	8.753	18.951	9.429	12.838
c	20.383	10.969	12.059	25.572	17.471	11.062	15.099	14.010
α	90.000	90.000	90.000	90.000	90.000	90.000	90.000	90.000
β	98.270	106.500	103.990	90.000	101.698	106.911	93.171	90.000
γ	90.000	90.000	90.000	90.000	90.000	90.000	90.000	90.000
U	1051.000	2145.9	2499.300	2060.100	3083.900	1598.900	1910.400	1785.000
D_x	1.369	1.407	1.197	1.472	1.158	1.306	1.302	1.162
Z	4	8	8	8	8	4	4	4
absorp coeff	0.328	0.100	0.073	0.107		0.086	0.091	0.064
space group	$P2_1/n$	$P2_1$	$P2_1/c$	$Pca2_1$	$C2/c$	$P2_1/n$	$P2_1/n$	$P2_12_12_1$

[a] Units: α, *β*, and *γ*, deg; *U*, Å^3; D_x, g/cm^3; absorption coefficient, cm^{-1}.

ranylidene)-2-pyrimidineamine:[32] mp 236−238 °C; ^{1}H NMR ($CDCl_3$) 9.33 (s, H), 8.84 (d, 2H), 7.29−8.40 (m, 6H).

***N*-(Diphenylethenylidene)benzeneamine (2a)** was obtained as bright yellow crystalline from phenyl isocyanate and (diphenylmethylene)triphenylphosphorane:[33] mp 55−56 °C; ^{1}H NMR ($CDCl_3$) 7.32−7.40 (m, Ar-H).

***N*-(Diphenylethenylidene)-4-nitrobenzeneamine (2b)** was obtained as a red crystal from triphenylphosphine, bromine, triethylamine, and *N*-(4-nitrophenyl)diphenylacetamide:[34] mp 84−86 °C; ^{1}H NMR ($CDCl_3$) 8.27 (d, 2H), 7.45 (d, 2H), 7.28−7.40 (m, 10H).

***N*-(Bis(4-methoxyphenyl)ethenylidene)-4-nitrobenzeneamine (2c)** was obtained using the same procedure for preparing **2a**. It was obtained as red crystals: mp 103.5−105.5 °C; ^{1}H NMR ($CDCl_3$) 6.92, 7.24 (2d, 8H), 7.44, 8.26 (2d, 4H), 3.82 (s, 6H).

***N*-(Diphenylethenylidene)-4-(*N*,*N*-dimethylamino)benzeneamine (2d)** was obtained using the same procedure for preparing **2a**. It was obtained as yellow crystals: mp 90−92 °C; ^{1}H NMR ($CDCl_3$) 6.69 (d, 2H), 7.20−7.36 (12H, m), 2.98 (s, 6H).

Acknowledgment. This work was supported by the National Science Foundation of China (Grants 29272070 and 29572074).

References and Notes

(1) (a) Streitweiser, A.; Heathcock, C. H. *Introduction to Organic Chemistry*; Macmillan: New York, 1985. (b) Neckers, D.; Doyle, M. P. *Organic Chemistry*; John Wiley: New York, 1977.

(2) Gould, E. S. *Mechanism and Structure in Organic Chemistry*; Holt-Dryden Book-Henry Holt and Co.: New York, 1960.

(3) (a) Zamir, S.; Bernstein, J.; Loffe, A.; Brunovll, J.; Kolonits, M.; Hargittai, I. *J. Chem. Soc., Perkin Trans. 2* **1994**, 895 and references cited therein. (b) Curtis, R. D.; Penner, G. H.; Power, W.; Wasylishen, R. E. *J. Phys. Chem*. **1990**, *94*, 400.

(4) (a) Skrabal, P.; Steiger, J. Zollinger, H. *Helv. Chim. Acta* **1975**, *58*, 800. (b) Bernstein, J.; Anderson, T. E.; Eckhardt, C. J. *J. Am. Chem. Soc*. **1979**, *101*, 541. (c) Patnaik, L. N.; Das, S. *Int. J. Quantum Chem*. **1985**, *27*, 135. (d) Akaba, R.; Tokumaru, K.; Kobayashi, T. *Bull. Chem. Soc. Jpn*. **1980**, *53*, 1993. (f) Akaba, R.; Sakuragi, H.; Tokumaru, K. *Bull. Chem. Soc. Jpn*. **1985**, *58*, 1186.

(5) Burgi, H. B.; Dunitz, J. D. *Helv. Chim. Acta* **1971**, *54*, 1255.

(6) (a) MÜller, M.; Hohlneicher, G. *J. Am. Chem. Soc.* **1990**, *112*, 1273. (b) Kendrick, J. *J. Chem. Soc., Faraday Trans*. **1990**, *86*, 3995.

(7) (a) Traetteberg, M.; Hilmo, I.; Hagen, K. *J. Mol. Struct.* **1977**, *39*, 231. (b) Traetteberg, M.; Frantsen, E. B.; Mijlhoff, F. C.; Hoekstra, A. *J. Mol. Struct*. **1975**, *26*, 57.

(8) Finder, C. J.; Newton, M. G.; Allinger, N. L. *Acta Crystallogr*. **1974**, *B30*, 411.

(9) Nakai, H.; Shiro, M.; Ezumi, K.; Sakata, S.; Kubota, T. *Acta Crystallogr.* **1976**, *B32*, 1827.

(10) Brown, C. J. *Acta Crystallogr*. **1966**, *21*, 146.

(11) Wiebcke, M.; Mootz, D. *Acta Crystallogr*. **1982**, *B38*, 2008.

(12) Stewart, J, J. P. *MOPAC*; Frank J. Seiler Research Laboratory, U.S. Air Force Academy, 1990; Version 6.

(13) (a) Bernstein, J.; Schmidt, G. M. *J. Chem. Soc., Perkin Trans. 2* **1972**, 951. (b) Bernstein, J.; Anderson,T. E.; Eckhardt, C. J. *J. Am. Chem. Soc.* **1979**, *101*, 541.

(14) Yu, Z. H. *Comput. Chem*. **1994**, *18*, 95.

(15) Kitaura, K.; Morokuma, K, *Int. J. Quantum Chem.* **1976**, *10*, 325.

(16) (a) Dewar, M. J. S.; Harget, A. J.; Trinajstic, N.; Worley, S. D. *Tetrahedron* **1970**, *26*, 4505. (b) Hess, B. S. A.; Schaad, L. S.; Holyoke, C. W. *Tetrahedron* **1975**, *31*, 295. (c) Katritzky, A. R.; Barczynski, P.; Musumarra, G.; Pisano, D.; Szafran, M. *J. Am. Chem. Soc*. **1989**, *111*, 7.

(17) Libit, L; Hoffmann, R. *J. Am. Chem. Soc*. **1974**, *96*, 1370.

(18) Kollmar, H. *J. Am. Chem. Soc.* **1979**, *101*, 4832.

(19) Dewar, M. J. S.; Dougherty, R. C. *The PMO Theory of Organic Chemistry*; Plenum Press: New York and London, 1975.

(20) (a) Cszmadia, I. G. *Molecular Structure and Conformation, Progress in Theoretical Organic Chemistry*; Elsevier: Amsterdam, 1982; Vol. 3. (b) Whangbo, M. H.; Schlegel, H. B.; Wolfe, S. *J. Am. Chem. Soc*. **1977**, *99*, 1296. (c) Kost, D.; Schlegel, H. B.; Mitchell, D. J.; Wolfe, S. *Can. J. Chem*. **1979**, *57*, 729.

(21) Müller, M.; Hohlneicher, G. *J. Am. Chem. Soc*. **1990**, *112*, 1273.

(22) Dewar, M. J. S. *The Molecular Orbital Theory of Organic Chemistry*; McGraw-Hill: New York, 1969; p 70.

(23) Bader, R. F. W.; Streitwieser, A.; Neuhaus, A.; Laidig, K. E.; Speers, P. *J. Am. Chem. Soc*. **1996**, *118*, 4959.

(24) (a) Hameka, H. F. *Advanced Quantum Chemistry*; Addison-Wesiey Publishing Co.: Reading, MA, 1965; p 75; (b) Musher, J. I.; Salem, L. *J. Chem. Phys.* **1966**, *44*, 2943. (c) Salem, L. *J. Am. Chem. Soc*. **1968**, *90*, 543. (d) Epiotis, N. D.; Cherry, W. R.; Shaik, S.; Yates, R.; Bernardi, F. In *Topics in Current Chemistry*; Springer: New York, 1977; Vol. 70, p 27.

(25) Csizmadia, I. G. *Theory and Practice of MO Calculation on Organic Molecules*; Elsevier: Amsterdam, 1976,

(26) Hiberty, P.C.; Danovich, D.; Shurki, A.; Shaik, S. *J. Am. Chem. Soc*. **1995**, *117*, 7760.

(27) Glendening, E. D.; Faust, R.; Streitwieser, A.; Vollhardt, K. P. C.; Weinhold, F. *J. Am. Chem. Soc*. **1993**, *115*, 10952.

(28) Shaik, S. S.; Hiberty, P. C.; Lefour, J. M.; Ohanessian, G. *J. Am. Chem. Soc*. **1987**, *109*, 363.

(29) (a) Wiberg, K. B.; Naksji, D.; Breneman, C. M. *J. Am. Chem. Soc.* **1989**, *111*, 4178. (b) Kistiakowsky, G. B.; Ruhoff, J. R.; Smith, H.A.; Vaughan, W. E. *J. Am. Chem. Soc.* **1935**, *57*, 876. (c) Streitwieser, A., Jr. *Molecular Orbital Theory for Organic Chemists*; Wiley: New York, 1961.

(30) (a) Epiotis, N. D. *Pure Appl. Chem.* **1983**, *55*, 229. (b) Epiotis, N. D. *Lecture Notes in Chemistry*; Springer-Verlag: New York, 1983; Vol. 34, p 360.

(31) (a) Hiberty, P. C.; Ohanessian, G.; Shaik, S. S.; Flament, J. P. *Pure Appl. Chem*. **1993**, *65*, 35. (b) Hiberty, P. C. *Topics in Current Chemistry*; Gutman, I., Cyrin, S. J., Eds.; Springer: New York, 1990; Vol. 153, p 27 and references cited therein. (c) Epiotis, N. D. *Nouv. J. Chim*. **1984**, *8*, 11.

(32) Bödeker, J.; Courault, K. *J. Prakt. Chem.* **1980**, S. 336.

(33) (a) Staudinger, H.; Meyer, J. *Chem. Ber*. **1920**, *53*, 72. (b) Froyen, P. *Acta Chem. Scand*. **1974**, *B28*, 586.

(34) (a) Bestmann, H. J.; Liener, J.; Mott, L. *Justus Liebigs Ann. Chem.* **1968**, *718*, 24. (b) Singhal, G. H.; Smith, H. Q. *J. Chem. Eng. Data* **1969**, *14*, 408.